RAPID COMMUNICATIONS

PHYSICAL REVIEW D

PARTICLES AND FIELDS

THIRD SERIES, VOLUME 48, NUMBER 7 1 OCTOBER 1993

RAPID COMMUNICATIONS

Rapid Communications are intended for important new results which deserve accelerated publication, and are therefore given priority in editorial processing and production. A Rapid Communication in **Physical Review D** *should be no longer than five printed pages and must be accompanied by an abstract. Page proofs are sent to authors, but because of the accelerated schedule, publication is generally not delayed for receipt of corrections unless requested by the author.*

Total cross section of the $pp \rightarrow pp\eta$ reaction near threshold

A. M. Bergdolt,[1] G. Bergdolt,[1] O. Bing,[1] A. Bouchakour,[1] F. Brochard,[1] F. Hibou,[1] A. Moalem,[1,2] A. Taleb,[1] M. P. Combes-Comets,[3] P. Courtat,[3] R. Gacougnolle,[3] Y. Le Bornec,[3] E. Loireleux,[3] F. Reide,[3] B. Tatischeff,[3] N. Willis,[3] M. Boivin,[4] B. M. K. Nefkens,[4,5] and F. Plouin[4]

[1]*Centre de Recherches Nucléaires, Université Louis Pasteur, B.P. 20, Institut National de Physique Nucléaire et de Physique des Particules–Centre National de la Recherche Scientifique, F-67037 Strasbourg CEDEX, France*

[2]*Department of Physics, Ben Gurion University, 84105 Beer Sheva, Israel*

[3]*Institut de Physique Nucléaire, F-91406 Orsay CEDEX, France*

[4]*Laboratoire National Saturne, Centre d'Etudes Nucléaires de Saclay, F-91191 Gif-sur-Yvette, France*

[5]*Department of Physics, University of California at Los Angeles, Los Angeles, California 90024*

(Received 25 January 1993)

The $pp \rightarrow pp\eta$ reaction is studied at energies near the η production threshold. The total cross sections at nominal machine energies of 1260, 1265, and 1300 MeV are 90±15, 790±120, and 3460±690 nb, respectively. None of the existing perturbative model calculations reproduces the energy dependence, which deviates strongly from phase space. This suggests that the cross section is enhanced in the near vicinity of the production threshold by a large η-pp scattering length.

PACS number(s): 13.75.Cs, 14.40.Aq, 25.40.Ve

It has long been expected, based on SU(6)⊗O(3) mixing, that the η-nucleon channel should couple strongly to the S_{11} (1535) resonance [1]. Now well established, this provides a motivation for studying η production [2–8] and forms the basis of several theoretical calculations [9–14]. In analogy to π production via an intermediate $\Delta(1232)$, η production proceeds through $XN \rightarrow S_{11}(1535) \rightarrow N\eta$, where a meson $X(\pi, \rho, \eta, \omega$, etc.) first produces an intermediate isobar, which decays subsequently into an ηN pair.

At LAMPF, coherent η production has been studied in $(\pi^{\pm}, \eta)$ reactions [3], whereas at the Saturne Synchrotron at Saclay effort has been concentrated on (p, η) reactions [4,8,15]. In particular, significant rates were found for the $pd \rightarrow {}^3\mathrm{He}\eta$ reaction at energies near the η threshold [2,4]. It has recently been demonstrated [5] that old $np \rightarrow dX$ data show a clear signal for $np \rightarrow d\eta$ with a total cross section $\sigma^{\max}_{np \rightarrow d\eta} = (110 \pm 15)\ \mu$b, corresponding to an isoscalar threshold amplitude, $|g_0| = 0.10 \pm 0.02$ fm^2. This value agrees reasonably well with a model [10] where the $S_{11}(1535)$ resonance is excited through the exchange of a ρ, π, and η. It is the purpose of the present work to report on a study of the isovector $pp \rightarrow pp\eta$ channel near threshold. The measurements already published were performed at much higher energies with rather poor statistics [16].

There is only one amplitude for the process $pp \rightarrow pp\eta$ near threshold, corresponding to the transition ${}^3P_0 \rightarrow {}^1S_0$ in the proton-proton system. In the center-of-mass (c.m.) frame,

$$f_{pp \rightarrow pp\eta} = g_1 \mathbf{p}_p^* \cdot \boldsymbol{\epsilon}_{pp} \ , \tag{1}$$

where g_1, $\mathbf{p}_p^*$, and $\boldsymbol{\epsilon}_{pp}$ denote the isovector amplitude, the momentum of the incoming proton, and the polarization vector of the two protons in the initial ${}^3P_0$ state. Following Ref. [11], the integrated cross section is written as

$$\sigma_{pp \rightarrow pp\eta} = 2\pi^2 p_p^* \int_0^{\sqrt{mQ_{\mathrm{c.m.}}}} p_\eta^* |g_1|^2 k^2 dk \ , \tag{2}$$

where m is the proton mass, p_η^* the momentum of the η in the overall c.m. frame, $2\mathbf{k}$ the relative momentum of the two final protons, and $Q_{\text{c.m.}}$ the energy above threshold in the c.m. system. All of these quantities can be determined by measuring the momenta of the outgoing protons. Using Eq. (2), the total cross section then allows us to extract a value of $\langle |g_1| \rangle$ averaged over k and p_η^*.

The measurements were performed at the Laboratoire National Saturne using the Saturne II accelerator. Proton beams of nominal energies 1260, 1265, and 1300 MeV were incident on a cryogenic H_2 target of thickness 398 ± 12 mg/cm^2. The beam intensity was monitored during the experiment by measuring the flux of particles, emitted from the target, using an ionization chamber and two telescopes, each composed of four scintillators. These monitors were stable over long time and were calibrated repeatedly during the experiment by carbon activation methods. Secondary particles were detected and analyzed in the SPES III spectrometer. At a nominal field of 3.1 T, its momentum acceptance is rather wide (600–1400 MeV/c) with a mean angular acceptance of 10^{-2} sr. The theoretical momentum resolution varies with the momentum between 4×10^{-4} and 10^{-3}. All the measurements reported here were performed with the spectrometer set at 0°. The large size of the detection system and wide momentum acceptance of the spectrometer are well adapted for experiments near threshold, where the outgoing particles (two protons in our case) fly in a narrow cone in the forward direction with small relative momenta and enter the spectrometer together.

The spectrometer is equipped with three multiwire drift chambers for particle tracking, the first of which (hereafter called MIT chamber) is located at the spectrometer focal plane. Two hodoscopes (A and B) $3m$ apart, each composed of 20 scintillators, serve as a trigger and provide time-of-flight measurements. Two additional hodoscope planes (C and D) placed between A and B reduce accidentals. (See Refs. [17, 18] for more details.) Particles are identified from time-of-flight measurements between pairs of A_iB_j scintillators. A two-particle event is recognized as a true coincidence if there are hits in two different A_iB_j pairs and two hits in the MIT chamber.

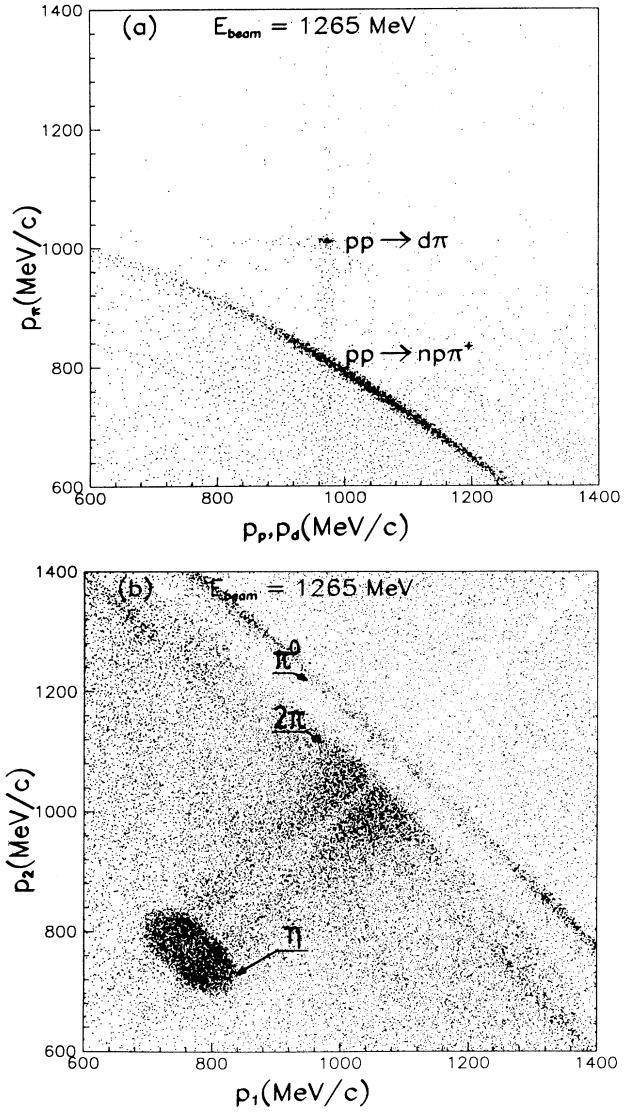

FIG. 1. Scatter diagrams of two particles in coincidence from measurements at $E_{\text{beam}}=1265$ MeV ($Q_{\text{c.m.}}=2.65$ MeV): (a) coincident π-proton and π-deuteron events only. The strong yield from the $pp\rightarrow pn\pi^+$ is due to the excitation of the Δ isobar. (b) Two proton events only. Near threshold there is no cut on momentum acceptance and the yield from η production appears as an ellipse.

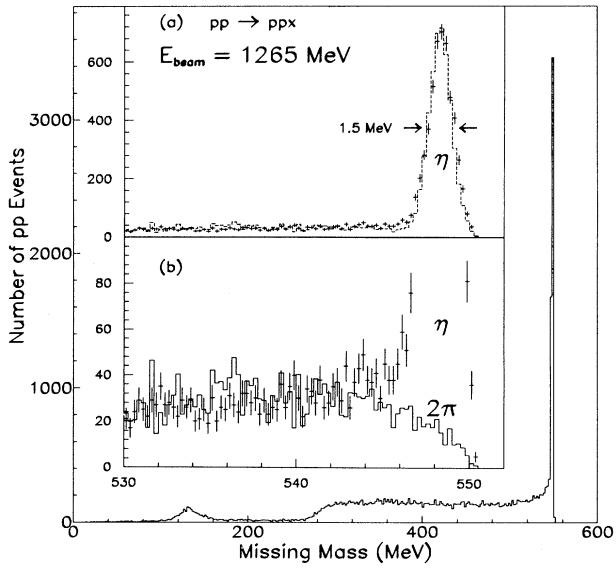

FIG. 2. Yield versus missing mass spectrum for two proton events corresponding to the scatter diagram Fig. 1(b). The FWHM resolution in the missing mass is about 1.5 MeV in the η-peak region. The insets display the fit to Monte Carlo simulations (solid and dashed curves) for (a) the η-peak region and (b) the background below and underneath the η peak. The shape of the yield below the η peak is well reproduced with two-pion production and its tail underneath the η peak provides a good estimate of the background contribution to the η-peak region (solid curve).

The detection system loses those events where (1) the two particles hit a common scintillator A_i (or B_j), (2) a particle passes in the dead zones between neighboring scintillators of the hodoscopes A,B,C,D, and (3) two particles travel close together at the focal plane and hence generate a single hit in the MIT chamber. All of these deficiencies are taken into account in the data reduction off line.

Typical scatter diagrams for two particles detected in coincidence are shown in Fig. 1. The loci of events corresponding to the $pp \rightarrow d\pi^+$, $pp \rightarrow pn\pi^+$ reactions [Fig. 1(a)] stand out clearly, as do the two-proton events $pp \rightarrow pp\pi^0$, $pp \rightarrow pp2\pi$, and $pp \rightarrow pp\eta$ reactions shown in Fig. 1(b). All of these reactions are measured and recorded simultaneously. In the case shown in Fig. 1(b), there are no losses of η events due to momentum acceptance and rather few due to angular acceptance, so that the η production yield appears as an ellipse. Events are, however, missing along the diagonal ($p_1 = p_2$), due mainly to two particles generating a single hit in the MIT chamber at the focal plane [category (3) above].

The counting rate versus missing mass spectrum is presented in Fig. 2. The resolution in missing mass is about 1.5 MeV [full width at half maximum (FWHM)] in the η peak region and at all energies studied, the η peak stands out clearly above the background. The resolution is considerably poorer for π^0's, mainly due to kinematics which, together with the imprecision in determining the momenta, have a greater effect for lower missing masses.

The cross section measurements are summarized in Table I. The spectra have been corrected by subtracting the target-empty contributions, though in the η-peak region, the target wall was responsible for only a few counts. The rates were also corrected for dead-time and counter efficiencies. All other corrections, arising from beam dispersion, the interactions in the target and counters, cuts on angular and momentum acceptance, and the trigger losses were included *via* a complete Monte Carlo simulation, details of which will be given elsewhere [19]. The yield from the $pp \rightarrow d\pi^+$, which was recorded simultaneously [see Fig. 1(a)], has served to verify the validity of these simulations and for beam energy calibration. All of the shapes of the d and π^+ peaks, the difference in their momenta, and the angular distributions at forward angles, were reproduced accurately, and the derived cross sections agreed within a few percent with those of Akemoto *et al.* [20]. The beam energy was determined by fitting the measured π and d momentum difference, $\Delta p = p_d - p_{\pi^+}$, to the predictions from the simulations. This procedure led to beam energies which are about 2.5 MeV lower than the nominal values mentioned above, a result previously found in Ref. [21]. The uncertainty in the beam energy is estimated to be less than 0.5 MeV. However, as the overall acceptance depends on the beam energy *and* η mass, the cross section in Table I is quoted versus $Q_{\text{c.m.}}$, the energy above threshold in the c.m. system. This quantity can be determined from the size of the η ellipse in Fig. 1(b) without making use of the beam energy calibration. In practice the values listed in Table I for $Q_{\text{c.m.}}$ (at midtarget) and their errors are deduced by fitting the measured and simulated spectra of the outgoing proton pair. At each energy χ^2 vs $Q_{\text{c.m.}}$ curves are generated and the $Q_{\text{c.m.}}$ value adopted corresponds to the minimal χ^2. The error in $Q_{\text{c.m.}}$ corresponds to the width of the curve at $\chi^2_{\min}+1$.

It is to be noted that the shape of the yield below the η peak is well reproduced by assuming two-pion production and the tail of this underneath the η peak provides a good estimate of the background contribution there. At incident energy of 1265 MeV the background to signal ratio is 1.5–2.0 %, which is similar to that reported for forward and backward production in the $pd \rightarrow {}^3\text{He}\,\eta$ reaction [4].

The total cross section errors quoted in Table I include statistical and systematic uncertainties in measuring the η number of counts (2–12 %), beam flux (8–11 %), the dead time (3%), the detector efficiencies (3–6 %), the target thickness (3%), and the overall acceptance as obtained from Monte Carlo simulations (10–12 %). At 1265 MeV ($Q_{\text{c.m.}} = 2.65$ MeV), measurements were undertaken with various vertical angular apertures. The fact that the cross section is nearly constant within the experimental errors, sustains our Monte Carlo simulations. At 1300 MeV ($Q_{\text{c.m.}} = 16.0$ MeV) the overall c.m. acceptance was smaller covering mainly $0.5 < |\cos\theta_{\text{c.m.}}| < 1.0$. The values quoted in Table I for the total cross sections are deduced from the Monte Carlo simulation assuming isotropic c.m. distributions, as would be expected for an s wave η with respect to the nucleon pair. Although this assumption could not be verified experimentally it is worth noting that the cross section from an independent measurement, which detected the η via its 2γ decay, is in fair agreement with our value at 1300 MeV [8].

The average isovector threshold amplitude g_1, derived from Eq. (2) and shown in Table I, falls by more than a factor of 3 between $Q_{\text{c.m.}} = 0.65$ MeV and $Q_{\text{c.m.}} = 16.0$ MeV. A similarly pronounced energy dependence was also deduced for the isoscalar amplitude from the shape of the $np \rightarrow d\eta$ energy spectrum [5]. Commonly, such strong variations occur when the final fragments of a reaction interact strongly and produce a resonance or a

TABLE I. Total cross section for the $pp \rightarrow pp\eta$. The first column is energy above threshold in the c.m. system as obtained from Monte Carlo simulations by fitting the size of the η ellipse. The values adopted correspond to the minimal χ^2; errors are the widths of the χ^2 vs $Q_{\text{c.m.}}$ curve at $\chi^2_{\min}+1$. The second column is the solid angle in the laboratory system. The third column is the background to signal ratio. The shape of the background underneath the η peak is taken from simulations of 2π production. The fourth column is the total cross section from at least two measurements. The adopted cross section at $Q_{\text{c.m.}} = 2.65$ MeV is 790±120 nb. The fifth column is taken from Eq. (2).

$Q_{\text{c.m.}}$ (MeV)	$\Delta\Omega$ (msr)	R (%)	$\langle\sigma_{pp\rightarrow pp\eta}\rangle$ (nb)	$\lvert g_1\rvert$ 10^{-2} fm$^{7/2}$
0.64±0.25	7.4	6.0	90±15	4.2±0.2
	3.9	1.5	840±130	
2.65±0.25	7.4	2.0	770±120	
	11.5	2.0	760±120	3.6±0.15
16.0±0.6	8.5	13.0	3460±690	1.3±0.2

bound state. The amplitude is consequently much larger than it would otherwise be, when the energy of the fragments approaches the resonance, and the cross section is enhanced. Using a similar parametrization in p_η^* to that in Ref. [5], our data require that the η-pp scattering length be of the order of 3 fm, which is fully consistent with the value deduced for the η-d [5] and somewhat smaller than η-^{3}He system [22].

Several authors have considered the $NN \rightarrow NN\eta$ through a perturbative approach [11–14] though none of them reproduced the energy dependence near threshold. In all of these model calculations, the predicted energy dependence is determined essentially by phase space. Germond and Wilkin [10] applied a one-boson-exchange model with the S_{11} mechanism dominating the reaction. There are large uncertainties in their predictions due to ambiguities in the relative phase of the π and ρ exchanges, and the magnitude of the ρNN^* coupling constant. With a ρNN^* coupling determined by vector dominance, the main contribution is due to the ρ. Their predictions for pure ρ exchange are given in Fig. 3 by the curve *GW*. The model requires that the relative phases of the π and ρ amplitudes should be opposite in the $np \rightarrow d\eta$ and the $pp \rightarrow pp\eta$ channels. This means that if the π and ρ amplitudes add constructively in g_0, they should interfere destructively in g_1. Such a solution, which is compatible with our results and with the single $np \rightarrow d\eta$ data point [5], can be obtained by reducing the ρNN^* coupling constant to 0.7 its value from vector dominance [10,11], and with the relative phases of the π, η, and ρ amplitudes taken to be $+$, $+$, and $-$, respectively. This solution (displayed by the curve *GWM* of Fig. 3) agrees well with our measurements at 1260 and 1265 MeV. The calculations in Ref. [11] were carried out to $Q_{\text{c.m.}} = 5$ MeV only.

Laget *et al.* [14] included the effects of the P_{11} and D_{13} resonances and could extend their calculations to higher energies. Their results (curve *LWLI* of Fig. 3), which correspond, in their formalism, to the π and ρ amplitudes summed constructively, are nearly identical to the *GWM*, but overestimate the cross section at 1300 MeV by more than a factor of 5. This is quite disturbing as the S_{11} mechanism should still be dominant at this energy though the effects of the p and d partial waves have been included [14]. The results corresponding to destructively interfering π and ρ exchange [23] are also given in Fig. 3 by the curve *LWLII*. It is identical in shape to *LWLI* but scaled down by a factor of about 5.5. It fits the cross section at 1300 MeV and is, in fact, very similar to the parametrization of De Paoli *et al.* [24] so that it should reproduce the cross sections at higher energies as well. It underestimates grossly, however, our results at lower energies, suggesting that the cross section is enhanced in the near vicinity of the η threshold. A similar pronounced energy dependence in the $pp \rightarrow pp\pi^0$ near threshold was shown to rise from the final state interaction between the outgoing protons [25]. In their calculations, Laget *et al.* [14,23] have included the interaction between the outgoing nucleons and therefore, the deviation reported above for the $pp \rightarrow pp\eta$ should be attributed to the interaction of the η with the nucleon pair. Finally, Vetter *et al.* [13] reported on similar model calculations. While they do agree with Refs. [11,14] that the S_{11} is dominant, they included ω exchange and assumed a rather small ρNN^* coupling. The calculated cross sections are much smaller than reported here, but the energy dependence is rather similar to the ones shown in Fig. 3.

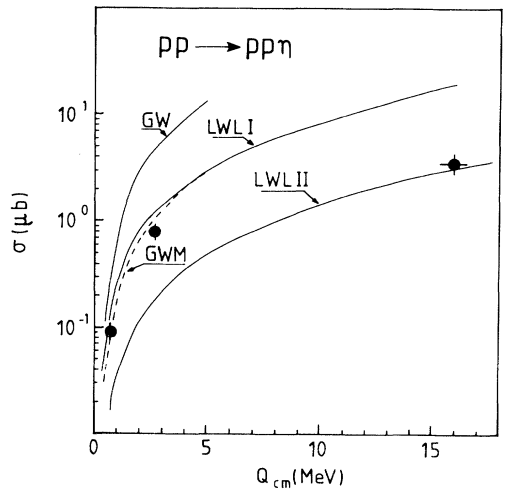

FIG. 3. Total cross section near threshold for the $pp \rightarrow pp\eta$ reaction. The data points are from the present measurements. Errors smaller than the data point size are not indicated. The curve *GW* is curve *d* of Ref. [11]. The curve *GWM* is deduced from this by (i) reducing their ρNN^* coupling by a factor of 0.7 and (ii) including contributions from π, η, and ρ exchanges with relative phases $+$, $+$, and $-$, respectively. The curves *LWLI* and *LWLII* are those of Refs. [14,23] with the π and the ρ amplitudes added constructively and destructively. All curves are drawn as a function of the c.m. Q value of the reaction to avoid effects due to different η-mass values used by the authors.

To conclude, the total cross section and isovector amplitude near threshold show a pronounced energy dependence which deviates strongly from phase space. None of the existing model calculations [11,14,23,13], which are based on the perturbative approach, accounts for the energy dependence near threshold. This is most probably due to neglecting final state interaction associated with a large η-pp scattering length.

We would like to thank C. Wilkin for reading the manuscript and for many useful suggestions. Discussions with J. M. Laget and communications are much appreciated. One of us (A.M.) would like to express his gratitude for the generous hospitality extended to him by the CNRS group of Strasbourg.

[1] See, for example, R. P. Feynman, M. Kislinger, and F. Ravndal, Phys. Rev. D **3**, 2706 (1971); R. Koniuk and N. Isgur, *ibid.* **21**, 1868 (1980).

[2] J. Berger *et al.*, Phys. Rev. Lett. **61**, 919 (1988).

[3] J. C. Peng *et al.*, Phys. Rev. Lett. **63**, 2353 (1989).

[4] F. Plouin *et al.*, in *Production and Decay of Light Meson*, Proceedings of the Workshop, Paris, France, 1988, edited by P. Fleury (World Scientific, Singapore, 1988).

[5] F. Plouin *et al.*, Phys. Rev. Lett. **65**, 690 (1990).
[6] J. Keyne *et al.*, Phys. Rev. D **14**, 28 (1976); H. Karami *et al.*, Nucl. Phys. **B276**, 503 (1979).
[7] M. Benmerrouche and N. C. Mukhopadhyay, Phys. Rev. Lett. **67**, 1070 (1991).
[8] G. Dellacasa *et al.*, Saturne Proposal No. 237 (unpublished); and (private communication).
[9] L. C. Liu, J. T. Londergan, and G. E. Walker, Phys. Rev. C **40**, 832 (1989).
[10] J. F. Germond and C. Wilkin, J. Phys. G **15**, 437 (1989).
[11] J. F. Germond and C. Wilkins, Nucl. Phys. **A518**, 308 (1990), and references therein.
[12] J. M. Laget and J. F. Lecolley, Phys. Rev. Lett. **61**, 2069 (1988).
[13] T. Vetter, A. Engel, T. Biro, and U. Mosel, Phys. Lett. B **263**, 153 (1991).
[14] J. M. Laget, F. Wellers, and J. F. Lecolley, Phys. Lett. B **257**, 254 (1991), and references therein.
[15] Y. Le Bornec *et al.*, Saturne Proposal No. 186 (unpublished).
[16] E. Pickup *et al.*, Phys. Rev. Lett. **8**, 329 (1962); L. Bodini *et al.*, Nuovo Cimento **A58**, 475 (1968); A. P. Colleraine and U. Nauenberg, Phys. Rev. **161**, 1387 (1967); G. Alexander *et al.*, *ibid.* **154**, 1284 (1967); C. Caso *et al.*, Nuovo Cimento **A55**, 66 (1968); R. R. Kinsey, Ph.D. thesis; E. Colton and E. Gellert, Phys. Rev. D **1**, 1979 (1970); G. Yekutieli *et al.*, Nucl. Phys. **B18**, 301 (1970); S. P. Almeida *et al.*, Phys. Rev. **174**, 1638 (1968); J. Le Guyarder *et al.*, Nucl. Phys. **B35**, 573 (1971).
[17] M. P. Combes-Comets *et al.*, Phys. Rev. C **43**, 973 (1991).
[18] E. Aslanides *et al.*, Nucl. Phys. **A528**, 608 (1991).
[19] A. M. Bergdolt *et al.* (unpublished).
[20] M. Akemoto *et al.*, Phys. Lett. **149B**, 321 (1984).
[21] F. Plouin *et al.*, Phys. Lett. B **276**, 526 (1992).
[22] C. Wilkin, Phys. Rev. C **47**, 938 (1993).
[23] J. J. Laget (private communication).
[24] A. De Paoli *et al.*, Phys. Lett. B **219**, 194 (1989).
[25] H. O. Meyer *et al.*, Nucl. Phys. **A539**, 633 (1992).